Assembling Phenomena of Calix[4]hydroquinone Nanotube Bundles by One-Dimensional Short Hydrogen Bonding and Displaced π−π Stacking

ARTICLE *in* JOURNAL OF THE AMERICAN CHEMICAL SOCIETY · OCTOBER 2002

Impact Factor: 12.11 · DOI: 10.1021/ja0259786 · Source: PubMed

J|A|C|S
ARTICLES
Published on Web 10/30/2002

Assembling Phenomena of Calix[4]hydroquinone Nanotube Bundles by One-Dimensional Short Hydrogen Bonding and Displaced $\pi-\pi$ Stacking

Kwang S. Kim,* Seung Bum Suh, Jong Chan Kim, Byung Hee Hong, Eun Cheol Lee, Sunggoo Yun, P. Tarakeshwar, Jin Yong Lee, Yukyung Kim, Hyejae Ihm, Heon Gon Kim, Jung Woo Lee, Jung Kyung Kim, Han Myoung Lee, Dongwook Kim, Chunzhi Cui, Suk Joo Youn, Hae Yong Chung, Hyuck Soon Choi,† Chi-Wan Lee,‡ Seung Joo Cho,§ Sukmin Jeong,|| and Jun-Hyung Cho⊥

Contribution from the National Creative Research Initiative Center for Superfunctional Materials and Department of Chemistry, Division of Molecular and Life Sciences, Pohang University of Science and Technology, San 31, Hyojadong, Namgu, Pohang 790-784, Korea

Received February 19, 2002

Abstract: Using the computer-aided molecular design approach, we recently reported the synthesis of calix[4]hydroquinone (CHQ) nanotube arrays self-assembled with infinitely long one-dimensional (1-D) short hydrogen bonds (H-bonds) and aromatic−aromatic interactions. Here, we assess various calculation methods employed for both the design of the CHQ nanotubes and the study of their assembly process. Our calculations include ab initio and density functional theories and first principles calculations using ultrasoft pseudopotential plane wave methods. The assembly phenomena predicted prior to the synthesis of the nanotubes and details of the refined structure and electronic properties obtained after the experimental characterization of the nanotube crystal are reported. For better characterization of intriguing 1-D short H-bonds and exemplary displaced $\pi-\pi$ stacks, the X-ray structures have been further refined with samples grown in different solvent conditions. Since X-ray structures do not contain the positions of H atoms, it is necessary to analyze the system using quantum theoretical calculations. The competition between H-bonding and displaced $\pi-\pi$ stacking in the assembling process has been clarified. The IR spectroscopic features and NMR chemical shifts of 1-D short H-bonds have been investigated both experimentally and theoretically. The dissection of the two most important interaction components leading to self-assembly processes would help design new functional materials and nanomaterials.

I. Introduction

Hollow tubular self-assembled structures based on organic molecules have attracted considerable attention because of their potential abilities for artificial biological channels, drug delivery, nanochemical reactors, and nano-organic materials.[1] The first stage of this type of research mainly focused on mimicking biological systems such as tubular transmembrane channels. Cyclic peptides and cyclodextrins have been used as tubular subunits to construct tubular assembled structures. However, natural tubular assemblies such as Tobacco mosaic virus are composed of nontubular subunits.[2] Very recently, we have reported self-assembling organic nanotubes composed of nontubular subunits of CHQ.[3] These nanotubes can be easily made thin and long and also in bundles. The self-assembled arrays of nanotubes were initially designed by computational methods. Now, the details of the computer-aided molecular design approach and the further refined theoretical results (after synthesis and X-ray and IR characterization of the organic nanotube bundles) are reported here. The details of the previous

* To whom correspondence should be addressed. E-mail: kim@postech.ac.kr.
† Present address: Department of Molecular Biology, The Scripps Research Institute, La Jolla, CA 92037, U.S.
‡ Present address: Department of Radiology, Radiopharmaceutical Chemistry Section, University of Pennsylvania Medical Center, Philadelphia, PA 19104, U.S.
§ Present address: Life Science Division, Korea Institute of Science and Technology, Seoul 130-650, Korea.
|| Present address: Department of Physics, Chonbuk National University, Chonju, Korea.
⊥ Present address: Department of Physics, University of Texas, Austin, TX 78712-1081, U.S.

(1) (a) Orr, W. G.; Barbour, L. J.; Atwood, J. L. *Science* **1999**, *285*, 1049−1052. (b) Harada, A.; Li, J.; Kamachi, M. *Nature* **1993**, *364*, 516−518. (c) Ghadiri, M. R.; Granja, J. R.; Milligan, R. A.; McRee, D. E.; Khazanovich, N. *Nature* **1993**, *366*, 324−327. (d) Feldman, Y.; Wasserman, E.; Srolovitz, D.; Tenne, R. *Science* **1995**, *267*, 222−225. (e) Ghadiri, M. R.; Granja, J. R.; Buehler, L. K. *Nature* **1994**, *369*, 301−304. (f) Aoyagi, M.; Biradha, K.; Fujita, M. *J. Am. Chem. Soc.* **1999**, *121*, 7457−7458. (g) Fenniri, H.; Mathivanan, P.; Vidale, K. L.; Sherman, D. M.; Hallenga, K.; Wood, K. V.; Stowell, J. G. *J. Am. Chem. Soc.* **2001**, *123*, 3854−3855. (h) Fenniri, H.; Deng, B.-L.; Ribbe, A. E.; Hallenga, K.; Jacob, J.; Thiyagarajan, P. *Proc. Natl. Acad. Sci. U.S.A.* **2002**, *99*, 6487−6492.
(2) Percec, V.; Ahn, C.-H.; Ungar, G.; Yeardley, D. J. P.; Moller, M.; Sheiko, S. S. *Nature* **1998**, *391*, 161−164.
(3) (a) Hong, B. H.; Lee, J. Y.; Lee, C.-W.; Kim, K. C.; Bae, S. C.; Kim, K. S. *J. Am. Chem. Soc.* **2001**, *123*, 10748−10749. (b) Hong, B. H.; Bae, S. C.; Lee, C.-W.; Jeong, S.; Kim, K. S. *Science* **2001**, *294*, 348−351. (c) Kim, K. S. *Cur. Appl. Phys.* **2002**, *2*, 65−69.

10.1021/ja0259786 CCC: $22.00

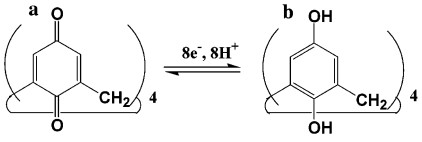

Figure 1. Schematic representation of (a) calix[4]quinone (CQ) and (b) calix[4]hydroquinone (CHQ). CQ can be electrochemically transferred to CHQ by accepting eight electrons and eight protons.

and the further refined experimental results (X-ray characterization, NMR chemical shifts, and IR spectroscopic analysis) are also added for a clear understanding of the intriguing structural and spectral features along with 1-D H-bonding and displaced $\pi-\pi$ stacking interactions. The 1-D H-bonds relay and the displaced $\pi-\pi$ stacks are quite interesting in that the intriguing features of 2-D and 3-D H-bonds have been reported recently[4] and the displaced versus edge-to-face $\pi-\pi$ interactions[5,6] have been an issue of intense interest. In particular, the study of competition between H-bonding and displaced $\pi-\pi$ stacking is extremely important because the two interactions are the most important interaction components leading to self-assembly processes.

CHQ is a reduced form of calix[4]quinone (CQ).[7] Quinone (Q) is one of the major electron/proton carriers in biological systems.[8] It can be simply reduced to hydroquinones (HQ) through electrochemical processes, as shown in Figure 1.[9] Although CQ and CHQ are likely to be similar in structure, their supramolecular structures and properties are clearly different because of the difference in chemical binding between carbonyl groups and hydroxyl groups. We have found that the "cone" structures of CHQs can form hollow tubular structures.

Several predictions on many interesting molecular systems have recently been made with ab initio calculations.[10] In this regard, we here show how the arrays of CHQ nanotubes have been designed from ab initio calculations so that this approach can be utilized to design other functional molecular systems. We have studied the relative energies of various conformers of CQ and CHQ and the difference in assembling phenomena of CHQs in the absence and presence of water molecules. We have investigated the competition between the 1-D short H-bonding and displaced $\pi-\pi$ stacking interactions in the assembling process of CHQ nanotube bundles. On the basis of first principles calculations of the self-assembled CHQ nanotube crystal, its electronic structure (including the density of states and the band gap) is discussed. In terms of computer-aided molecular design approach, we have tried to assess the suitability of various computational methods that were employed for the design of functional molecular systems and the investigation of assembly phenomena.

In biochemical problems, in particular, in enzymatic mechanisms, short strong H-bonds (SSHBs) have been an important issue.[11,12] While SSHBs are known to appear in charged systems (in particular, in anionic systems with oxyanions around a H atom), the present short H-bonds appear in noncharged systems. Therefore, the study of this type of H-bond strength is very intriguing. In addition, the study of fantastically well-ordered displaced $\pi-\pi$ stacks present in the CHQ nanotube bundles is very interesting. Thus, for better characterization of the CHQ structure, we have added herein X-ray analysis of the CHQ crystals grown in a different condition from the previously reported crystal. IR spectroscopic characterization for 1-D short H-bonds is of importance, and this experiment has been carried out along with normal-mode analysis. The NMR chemical shifts for the cone region comprised of four O−H groups H-bonded in the CHQ monomer have been investigated both experimentally and theoretically, and the chemical shifts for the short H-bonds are predicted.

II. Theoretical and Experimental Methods

We have carried out theoretical investigation of the CHQ nanotube systems to understand the assembly process as well as the geometrical and electronic structures. Initial conformational studies for the assembly process were carried out using molecular mechanics and molecular dynamics (MD). In this case, many existing force parameters were not useful for predicting reasonably correct conformers. The next step was to employ semiempirical methods (such as PM3),[13] which provided useful initial geometries of various conformers. Then, the density functional calculations were employed using Becke three parameters with Lee−Yang−Parr functionals (B3LYP), first with small basis set (3-21G) and followed by a reasonable size of the basis set (6-31G*). For better accuracy, we also carried out Moller Plesset second-order perturbation (MP2) calculations using 6-31G* and aug-cc-pVDZ basis sets for the comparison between H-bonds and $\pi-\pi$ stacking interactions, wherever the dispersion energy should be seriously considered (in particular, in the $\pi-\pi$ stacking interactions). The B3LYP and MP2 calculations were carried out using a Gaussian suite of programs.[14] All structures were fully optimized at all levels of theory unless otherwise specified. Large calculations in the present system include up to 4704 basis functions (in the octamer including bridging water molecules), which would be one of the largest calculations reported so far. We also carried out pseudopotential plane wave density functional theory (PW-DFT) calculations for the periodic crystal systems, which have been employed in condensed matter systems.[15,16] For PW-DFT calculation of CHQ nanotubes, we have used a generalized gradient approximation (GGA) of Perdew and Wang[17] and Vanderbilt pseudo-

(4) (a) Gong, B.; Cheng, C.; Skrzypczak-Jankun, E.; Yan, Y.; Zhang, J. *J. Am. Chem. Soc.* **1998**, *120*, 11194−11195. (b) Clegg, R. S.; Reed, S. M.; Hutchinson, J. E. *J. Am. Chem. Soc.* **1998**, *120*, 2486−2487.
(5) (a) Burley, S. K.; Petsko, G. A. *Science* **1985**, *229*, 23−28. (b) Hunter, C. A. *Chem. Soc. Rev.* **1994**, *23*, 101−109. (c) Tarakeshwar, P.; Choi, H. S.; Kim, K. S. *J. Am. Chem. Soc.* **2001**, *123*, 3323−3331. (d) Engkvist, O.; Hobza, P.; Selzle, H. L.; Schlag, E. W. *J. Chem. Phys.* **1999**, *110*, 5758−5762. (e) Hong, B. H.; Lee, J. Y.; Cho, S. J.; Yun, S.; Kim, K. S. *J. Org. Chem.* **1999**, *64*, 5661−5665. (f) Ren, T.; Jin, Y.; Kim, K. S.; Kim, D. H. *J. Biomol. Struct. Dyn.* **1997**, *15*, 401−405.
(6) Kim, K. S.; Tarakeshwar, P.; Lee, J. Y. *Chem. Rev.* **2000**, *100*, 4145−4186.
(7) (a) Morita, Y.; Agawa, T.; Nomura, E.; Taniguchi, H. *J. Org. Chem.* **1992**, *57*, 3658−3662. (b) Gometz-Kaifer, M.; Reddy, P. A.; Gutsche, C. D.; Echegoyen, L. *J. Am. Chem. Soc.* **1994**, *116*, 3580−3587.
(8) Stowell, M. H. B.; McPhillips, T. M.; Rees, D. C.; Soltis, S. M.; Abresch, E.; Feher, G. *Science* **1997**, *276*, 812−816.
(9) Gupta, N.; Linschitz, H. *J. Am. Chem. Soc.* **1997**, *119*, 6384−6391.
(10) (a) Urnezius, E.; Brennessel, W. W.; Cramer, C. J.; Ellis, J. E.; Schleyer, P. v. R. *Science* **2002**, *295*, 832−834. (b) Wu, Y.-D.; Zhao, Y.-L. *J. Am. Chem. Soc.* **2001**, *123*, 5313−5319. (c) de Visser, S. P.; Ogliaro, F.; Harris, N.; Shaik, S. *J. Am. Chem. Soc.* **2001**, *123*, 3037−3047. (d) Son, H. S.; Hong, B. H.; Lee, C.-W.; Yun, S.; Kim, K. S. *J. Am. Chem. Soc.* **2001**, *123*, 514−515. (e) Woodcock, H. L.; Moran, D.; Schleyer, P. v. R.; Schaefer, H. F. *J. Am. Chem. Soc.* **2001**, *123*, 4331−4335. (f) Raymo, F. M.; Bartberger, M. D.; Houk, K. N.; Stoddart, J. F. *J. Am. Chem. Soc.* **2001**, *123*, 9264−9267. (g) Florian, J.; Leszczynski, J. *J. Am. Chem. Soc.* **1996**, *118*, 3010−3017. (h) Hrovat, D. A.; Chen, J.; Houk, K. N.; Borden, W. T. *J. Am. Chem. Soc.* **2000**, *122*, 7456−7460. (i) Oh, K. S.; Yoon, J.; Kim, K. S. *J. Phys. Chem. B* **2001**, *105*, 9726−9731.
(11) (a) Cleland, W. W.; Kreevoy, M. M. *Science* **1994**, *264*, 1887−1890. (b) Gerlt, J. A.; Grassman, P. G. *J. Am. Chem. Soc.* **1993**, *115*, 11552−11568. (c) Frey, P. A.; Whitt, S. A.; Tobin, J. B. *Science* **1994**, *264*, 1927−1930. (d) Lin, J.; Frey, P. A. *J. Am. Chem. Soc.* **2000**, *122*, 11258−11259.
(12) (a) Kim, K. S.; Oh, K. S.; Lee, J. Y. *Proc. Natl. Acad. Sci. U.S.A.* **2000**, *97*, 6373−6378. (b) Kim, K. S.; Kim, D.; Lee, J. Y.; Tarakeshwar, P.; Oh, K. S. *Biochemistry* **2002**, *41*, 5300−5306. (c) Oh, K. S.; Cha, S.-S.; Kim, D.-H.; Cho, H.-S.; Ha, N.-C.; Choi, G.; Lee, J. Y.; Tarakeshwar, P.; Son, H. S.; Choi, K. Y.; Oh, B.-H.; Kim, K. S. *Biochemistry* **2000**, *39*, 13891−13896. (d) Cho, H. S.; Ha, N.-C.; Choi, G.; Kim, H.-J.; Lee, D.; Oh, K. S.; Kim, K. S.; Lee, W.; Choi, K. Y.; Oh, B.-H. *J. Biol. Chem.* **1999**, *274*, 32863−32868.
(13) Stewart, J. J. P. *J. Comput. Chem.* **1989**, *10*, 209−220; 221−264.

potential.[18] The cutoff energy of the plane wave basis set is 20 Ry. PW-DFT is free from basis set superposition error (BSSE) because plane wave basis sets cover all the space almost uniformly unlike the Gaussian orbitals spanning only a local region. The whole molecular structure in the X-ray crystal unit cell was fully optimized with the periodic boundary condition.

In the present system, PM3 results show very poor reliability. Nevertheless, they provide preliminary structures of informative conformers and suggest a possible trend. However, the interpretation of the results should be done with very careful discretion. In B3LYP/3-21G, bond distances are underestimated, and binding energies are overestimated, and so the BSSE-corrected binding energies are more realistic. Nevertheless, the trend observed for different chemical systems is somewhat reliable. In our calculations, the BSSE correction was made using the counterpoise method. The B3LYP/6-31G* method is reliable in most cases in predicting both structures and binding energies, while the computation time is not highly demanding unlike MP2 calculations. Thus, B3LYP/6-31G* method is recommended for computer-aided design approach for prediction of functional molecular systems and investigation of self-assembling phenomena. Nevertheless, the B3LYP method cannot properly take into account the $\pi-\pi$ interactions. The strong and weak points of each calculation method can be assessed from our results, which will be discussed later. Most of the molecular figures and vibrational modes were drawn using Pohang Sci-Tech Molecular Modeling package (POSMOL).[19]

To characterize the structures of CHQ tube bundles, we carried out further X-ray analysis grown in different conditions. In addition to the previous CHQ crystal grown in cesium sulfate, we here added the X-ray characterization of the CHQ crystal grown in the tetramethylammonium hexafluorophosphate. Both crystals have almost the same structures. In our following discussion, we use the average values of the two results. The X-ray structures have been used not only to assess the calculation methods but also to understand the features of 1-D H-bonding and displaced $\pi-\pi$ stacking.

For the analysis of 1-D short H-bonds and four-membered circular H-bonds in the cone structure of CHQ, we carried out IR spectral analysis of the CHQ monomer and CHQ nanotubes, using IR spectrometers along with the normal-mode analysis based on the B3LYP/6-31G* predicted spectra. In addition, we obtained the proton chemical shifts (using 500 MHz NMR; DRX500, Bruker) and compared these experimental data with the calculated values on the basis of the gauge independent atomic orbital (GIAO) method. In this case, Hartree−Fock (HF) results (than B3LYP calculations) were employed for better agreements with the experimental data.

III. Results

A. Calix[4]quinone Versus Calix[4]hydroquinone. According to ab initio calculations, the most stable conformers of CQ and CHQ are "partial cone" (Figure 2b) and "cone" (Figure 2a′) structures, respectively, which are in agreement with experiments (Table 1).

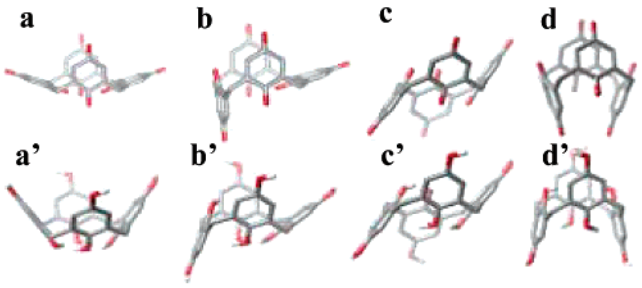

Figure 2. Four stable conformers of calix[4]quinone (top figures) and calix[4]hydroquinone (bottom figures): (a,a′) cone, (b,b′) partial cone, (c,c′) 1,2-alternative, and (d,d′) 1,3-alternative.

Table 1. Calculated Complexation Energies (B3LYP/6-31G*) of the Four Stable Conformers of the CQ Monomer and CHQ Monomer (kcal/mol)[a]

	cone	partial cone	1,2-alternate	1,3-alternate
CQ	1.8	0*	7.7	0.7
CHQ	0*	11.6	18.3	19.8

[a] All the energies are relative to the most stable conformers marked with an asterisk. The most stable conformer of CHQ is in accordance with the crystal structure.[3]

CHQ is composed of four hydroquinones; therefore, it has eight hydroxyl groups. Among them, four inner hydroxyl groups form a circular proton-tunneling resonance of H-bonds[20] which stabilize the "cone" structures, and the other four hydroxyl groups in the upper rim of the cone have dangling H atoms, which make it possible to form intermolecular H-bonds that lead to self-assembled structures. We have two well-refined X-ray data sets: X-ray1 which was based on the crystal grown in the presence of Cs_2SO_4 and X-ray2 which was based on the crystal grown in the presence of NMe_4PF_6 (Supplementary Information). We will compare our calculated structures with the average values of the two X-ray data sets ($X\text{-}ray_{av}$). The brief information of the X-ray characterization is given in the footnote of Table 2. The experimental (X-ray) and calculated (B3LYP/6-31G*) structures of the CHQ monomer are in excellent agreement (within 0.01 Å in bond lengths and 3 degrees in bond/torsional angles) (Table 2). PW-DFT results are also in good agreement with the X-ray data (within 0.01 Å in bond lengths and 4 degrees in bond/torsional angles), while the H-bond distance (O···O) is slightly shorter (by 0.08 Å in the monomer calculation and 0.06 Å in the crystal calculation) than but still in good agreement with the X-ray value. There is no significant difference between two PW-DFT results of the monomer and crystal calculations except for the drastically increased O−H bond lengths on the rim of the CHQ monomer (1.018 Å) in the crystal calculation due to the short H-bonding. These lengths are slightly longer than those in the cone region (comprised of four O−H groups H-bonded as a ring) of the CHQ monomer (1.011 Å). The former and the latter are longer than the non-hydrogen bonded length (0.970 Å) by 0.048 and 0.041 Å, respectively. This would indicate that the short H-bond along the CHQ tubular axis would be stronger in H-bond strength than the H-bond in the cone.

(14) Frisch, M. J.; Trucks, G. W.; Schlegel, H. B.; Scuseria, G. E.; Robb, M. A.; Cheeseman, J. R.; Zakrzewski, V. G.; Montgomery, J. A., Jr.; Stratmann, R. E.; Burant, J. C.; Dapprich, S.; Millam, J. M.; Daniels, A. D.; Kudin, K. N.; Strain, M. C.; Farkas, O.; Tomasi, J.; Barone, V.; Cossi, M.; Cammi, R.; Mennucci, B.; Pomelli, C.; Adamo, C.; Clifford, S.; Ochterski, J.; Petersson, G. A.; Ayala, P. Y.; Cui, Q.; Morokuma, K.; Malick, D. K.; Rabuck, A. D.; Raghavachari, K.; Foresman, J. B.; Cioslowski, J.; Ortiz, J. V.; Baboul, A. G.; Stefanov, B. B.; Liu, G.; Liashenko, A.; Piskorz, P.; Komaromi, I.; Gomperts, R.; Martin, R. L.; Fox, D. J.; Keith, T.; Al-Laham, M. A.; Peng, C. Y.; Nanayakkara, A.; Gonzalez, C.; Challacombe, M.; Gill, P. M. W.; Johnson, B. G.; Chen, W.; Wong, M. W.; Andres, J. L.; Head-Gordon, M.; Replogle, E. S.; Pople, J. A. Gaussian 98; Gaussian, Inc.: Pittsburgh, PA, 1998.
(15) (a) Cho, J.-H.; Kleinman, L.; Chan, C. T.; Kim, K. S. *Phys. Rev. B* **2001**, *63*, 073306-1-4. (b) Cho, J.-H.; Kim, K. S. *Phys. Rev. B* **2000**, *62*, 1607−1610.
(16) Kresse, G.; Furthmuller, J. *Phys. Rev. B* **1996**, *54*, 11169−11186.
(17) (a) Wang, Y.; Perdew, J. P. *Phys. Rev. B* **1991**, *43*, 8911−8916. (b) Perdew, J. P.; Wang, Y. *Phys. Rev. B* **1992**, *45*, 13244−13249. (c) Ceperley, D. M.; Alder, B. J. *Phys. Rev. Lett.* **1980**, *45*, 566−569.
(18) Vanderbilt, D. *Phys. Rev. B* **1990**, *41*, 7892−7895.
(19) Lee, S. J.; Kim, K. S. POSMOL (Reg. No. 2000-01-12-4239), Postech Licensing Center, Pohang, Korea, 2000. (Anonymous ftp address: ftp://csm50.postech.ac.kr/posmol)
(20) (a) Brougham, D. F.; Caciuffo, R.; Horsewill, A. J. *Nature* **1999**, *397*, 241−243. (b) Horsewill, A. J.; Jones, N. H.; Caciuffo, R. *Science* **2001**, *291*, 100−103.

Table 2. X-ray and Calculated Structures of the Cone-Shaped CHQ Monomer[a]

	O···O	O–H_c	O–H_r	OHO	O–C_c	O–C_r	C_r–C	C_c–C	C–C	C–C_m	OO O	O···O–C	O···O···O–C
X-ray1[b]	2.667	(0.83)	(0.83)		1.391	1.376	1.385	1.397	1.388	1.518	90.0	111.0,113.0	−112.9, −114.7
X-ray2[c]	2.654	(0.82)	(0.82)		1.391	1.377	1.379	1.395	1.387	1.511	90.0	110.6,113.3	−112.5, −114.9
X-ray_{av}[d]	2.661	(0.83)	(0.83)		1.391	1.377	1.382	1.396	1.388	1.515	90.0	110.8, 113.2	−112.7, −114.8
B3LYP/ 6-31G*[e]	2.668	0.993	0.970	165.5	1.386	1.371	1.395	1.405	1.398	1.526	90.0	114.9	−112.4
PW-DFT (monomer)	2.582	1.013	0.970	166.9	1.397	1.382	1.393	1.404	1.397	1.518	90.0	111.8	−117.6
PW-DFT (crystal)	2.599	1.011	1.018	167.0	1.397	1.384	1.392	1.401	1.396	1.513	90.0	114.0, 116.2	−112.0, −113.8

[a] Bond distances (Å) in the cases of two atoms, bond angles (degree) in the cases of three atoms, and torsional angles (degree) in the case of four atoms. Subscripts "c", "r", and "m", denote the cone position, rim position, and methylene carbon position of the cone-shape CHQ monomer, respectively. The B3LYP/6-31G* results were based on the isolated pure monomer, while the PW-DFT results were based on both the monomer and the predicted CHQ crystal structure. The X-ray O−H bond lengths were obtained from the time-averaged electron density; thus, these nondynamic values are not accurate enough because of the lack of consideration of high mobility of H atoms. The structure of the monomer moiety shows C_2 symmetry (only slightly off C_4 symmetry). Although the bond distances were averaged, two different angles were not averaged to show C_2 symmetry. The B3LYP and PW-DFT structures for the monomer show C_4 symmetry. However, for the PW-DFT structure of the crystal, the monomer moiety shows C_2 symmetry with two slightly different types of H-bonded O···O distances possibly because of the short H-bonding and $\pi-\pi$ stacking interactions. Here, the average value of the O···O distances is reported, as in the X-ray data. [b] Crystal data grown in Cs_2SO_4: orthorhombic, space group C_{mmm} with a = 23.3007(5) Å, b = 25.03569(10) Å, c = 11.6313(2) Å, and $\alpha = \beta = \gamma = 90°$ for empirical formula $C_{28}H_{32}O_{12}$; V = 6785.08(19) $Å^3$, Z = 8, T = 223(2) K. Final full matrix least-squares refinement on F^2 with all 2988 reflections and 230 variables converged to R1($I > 2\sigma(I)$) = 0.0808, wR2(all data) = 0.2602. The present result is the refined one of the original X-ray data which did not include highly refined solvent water structure. The previous X-ray data were deposited in the Cambridge Crystallographic Data Centre as supplementary publication no. CCDC-161593. [c] Crystal data grown in NMe_4PF_6: orthorhombic, space group C_{mmm} with a = 23.365(3) Å, b = 24.914(3) Å, c = 11.5852(16) Å, and $\alpha = \beta = \gamma = 90°$ for empirical formula $C_{28}H_{32}O_{12}$; V = 6743.7(16) $Å^3$, Z = 8, T = 293(2) K. Final full matrix least-squares refinement on F^2 with all 2703 reflections and 230 variables converged to R1($I > 2s(I)$) = 0.0816, wR2(all data) = 0.2435. [d] Average value of the two sets of X-ray data. [e] Calculation of the CHQ monomer.

Table 3. Experimental and Calculated Chemical Shifts (δ in ppm) of the Cone-Shaped CHQ Monomer[a]

CHQ (Figure 3)	$OH_{c\ one}$	OH_{rim}	CH	CH_2
expt: CHQ in acetone−water				
	9.83	7.81	6.64	4.06, 3.50
calcd: CHQ monomer				
B3LYP/6-31G*	8.65	3.16	5.93, 6.32	3.98, 3.08
HF//B3LYP/6-31G*	9.37	3.47	6.43, 6.93	4.11, 3.24
calcd: CHQ monomer +4(H_2O)				
HF//B3LYP/6-31G*	8.71	7.40	6.61, 7.29	3.97, 3.12

To facilitate our discussion of the comparison between the CHQ monomer and nanotubes, we report both experimental and calculated chemical shifts (δ in ppm) for the CHQ monomer (Table 3 and Figure 3). The experimental data was obtained in the presence of acetone and water, while the calculations were done both in the absence of water and in the presence of four microsolvated water molecules. The B3LYP/6-31G* calculations tend to slightly underestimate the chemical shifts, while the HF/6-31G*//B3LYP/6-31G* gives realistic values close to the experimental ones. This trend was well noted in our previous study of chemical shifts of SSHBs in enzymes.[12a] The present results for the microsolvation of the CHQ monomer match well the experimental chemical shifts of OHs at the upper rim.

B. Self-Assembly of Calix[4]hydroquinone. In the first stage of the self-assembling study of CHQs, we carried out ab initio calculations for various possible combinations of assembled structures derived from previously reported calixarene-based dimers,[21] trimers,[22] tertramers,[23] hexamers,[24] and polymers.[25] In the *n*-oligomer, the number of OH groups is 8*n*, and thus, 4*n* OH groups form *n* cones comprised of four-membered circular H-bonds, and thus the remaining 4*n* OH groups can involve intermolecular H-bonds. All the dangling H atoms in the *n*-oligomer (comprised of *n* monomers) can form up to 4*n*

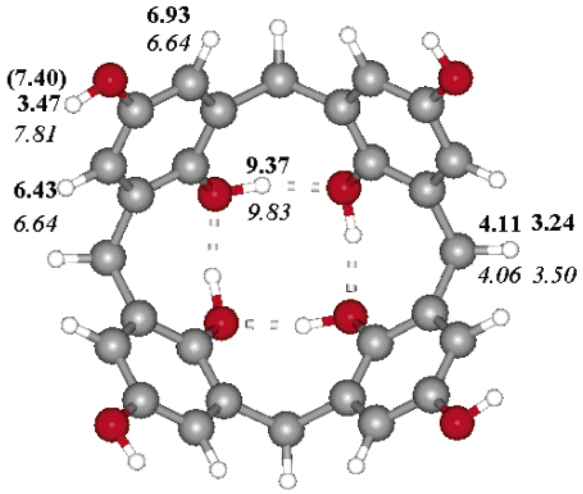

Figure 3. HF//B3LYP/6-31G* (in bold) and experimental (in italic) chemical shifts (in ppm) of the cone-shaped CHQ monomer. The experimental values of the CHQ monomers were obtained in the acetone−water solution. The value in parentheses is the calculated value by microsolvation of the CHQ monomer by four water molecules (Table 3).

H-bonds. However, in the dimer structure (Figure 4a), CHQs form a capsule connected by only 4 H-bonds. Likewise, trimer (Figure 4b) and tetramer (Figure 4c) have 6 and 8 H-bonds to form cyclic structures, and the tubular octamer (Figure 3e) has 16 H-bonds. On the other hand, the octahedral hexamer (Figure 4d) forms 24 H-bonds with no dangling H atoms. The calculated assembling energies per monomer of the dimer, trimer, tetramer, hexamer, and octamer (Figure 4a−e) at the BSSE-uncorrected B3LYP/6-31G*//B3LYP/3-21G level are 9, 8, 9, 21, and 11 kcal/mol, respectively, and those of dimer, trimer, tetramer, and hexamer at the 50%-BSSE-corrected[6,26,27] B3LYP/6-31G* level are 10, 9, 9, 22 kcal/mol, respectively (Table 4).[28] This indicates that the hexamer (Figure 4d) is the most favorable self-assembling structure because of full saturation of the dangling H atoms by H-bonding. The numbers of the dangling H atoms

(21) Kikuchi, Y.; Tanaka, Y.; Sutarto, S.; Kobayashi, K.; Toi, H.; Aoyama, Y. *J. Am. Chem. Soc.* **1992**, *114*, 10302−10306.
(22) Prins, L. J.; Jong, F. D.; Timmerman, P.; Reinhoudt, D. N. *Nature* **2000**, *408*, 181−184.
(23) Chopra, N.; Sherman, J. C. *Angew. Chem., Int. Ed. Engl.* **1997**, *36*, 1727−1729.
(24) MacGillivray, L. R.; Atwood, J. L. *Nature* **1997**, *389*, 469−472.
(25) Castellano, R. K.; Rudkevich, D. M.; Rebek, J., Jr. *Proc. Natl. Acad. Sci. U.S.A.* **1997**, *94*, 7132−7137.
(26) Kim, J.; Kim, K. S. *J. Chem. Phys.* **1998**, *109*, 5886−5895.
(27) (a) Kim, J.; Lee, S.; Cho, S. J.; Mhin, B. J.; Kim, K. S. *J. Chem. Phys.* **1995**, *102*, 839−849. (b) Kim, J.; Kim, K. S. *J. Chem. Phys.* **2000**, *113*, 5259−5272. (c) Lee, H. M.; Suh, S. B.; Lee, J. Y.; Tarakeshwar, P.; Kim, K. S. *J. Chem. Phys.* **2000**, *112*, 9759−9772.

Table 4. Calculated Assembling Energy of CHQ Oligomers (kcal/mol per CHQ Monomer)[a]

without water	a. dimer (C_2)	b. trimer (D_3)	c. tetramer (D_4)	d. hexamer (O_h)	e. octamer* (S_4)
PM3	−5.1	−3.7	−6.3	−11.2	−11.5
B3LYP/3-21G	−28.2 (−8.7)	−20.7 (−8.2)	−23.2 (−12.0)	−51.2 (−29.6)	−34.2 (−14.6)
B3LYP/6-31G*//B3LYP/3-21G	−9.2	−8.3	−9.4	−21.1	−11.0
B3LYP/6-31G*	−13.1 (−7.2)	−10.5 (−6.7)	−10.7 (−7.0)	−24.6 (−18.7)	
	−10.2 ± 2.9	−8.6 ± 1.9	−8.8 ± 1.9	−21.6 ± 3.0	
with water (symmetry)	**a′. dimer+4W (C_2)**	**b′. trimer+6W (D_3)**	**c′. tetramer+8W (D_4)**	**d′.(=d) hexamer (O_h)**	**e′. octamer+16W* (S_4)**
PM3	−19.8	−10.7	−19.2	−11.2	−23.8
B3LYP/3-21G	−117.0 (−58.1)	94.8 (−44.9)	−90.0 (−39.9)	−51.2 (−29.6)	−115.4 (−61.3)
B3LYP/6-31G*//B3LYP/3-21G	−37.3	−35.9	−31.9	−21.1	−37.5
B3LYP/6-31G*	−52.7 (−35.8)	−46.6 (−32.8)	−43.9 (−31.0)	−24.6 (−18.7)	−54.1 (−40.3)
	−44.2 ± 8.4	−39.7 ± 6.9	−37.4 ± 6.4	−21.6 ± 3.0	−47.2 ± 6.9

[a] Energies are in kcal/mol per CHQ monomer. Each *n*-mer has 8*n* OH groups among which 4*n* OH groups form four-membered circular H-bonds in each cone. In the absence of water, *n*-mer involves 2*n* H-bonds with 2*n* OH groups. The remaining 2*n* OH groups can involve intermolecular H-bonds. If these OH groups do not involve in intermolecular H-bonding, they form H-bonds with bridging water molecules in the presence of water. Full BSSE-corrected energies are reported in parentheses. In B3LYP/ 6-31G*, the interaction energies are also given in the second line as a median value between BSSE-uncorrected and BSSE-corrected values with the error bar of 50%-BSSE.[6,26,27] Thus, for each reported value, the lower bound is the BSSE-uncorrected value, and the upper value is the BSSE-corrected value.

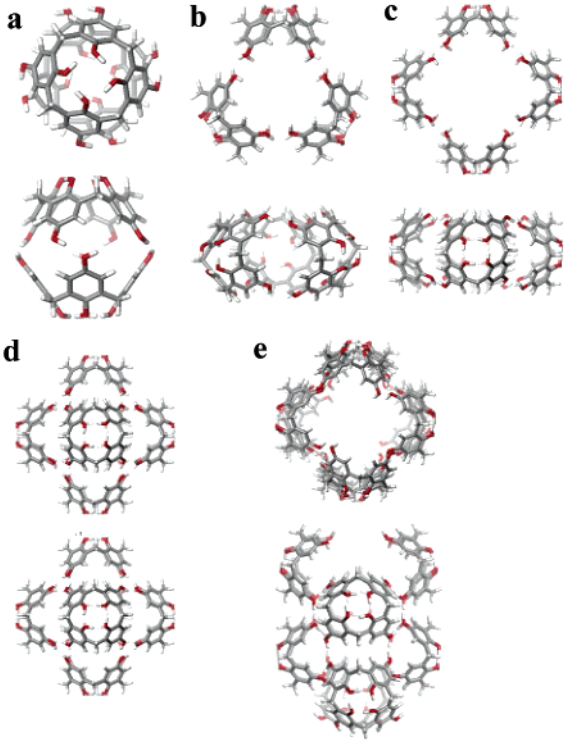

Figure 4. Calculated structures of *n*-oligomers in the absence of water molecules (top and side views): (a) CHQ dimer, (b) trimer, (c) tetramer, (d) octahedral hexamer, and (e) tubular octamer (B3LYP/6-31G* level).

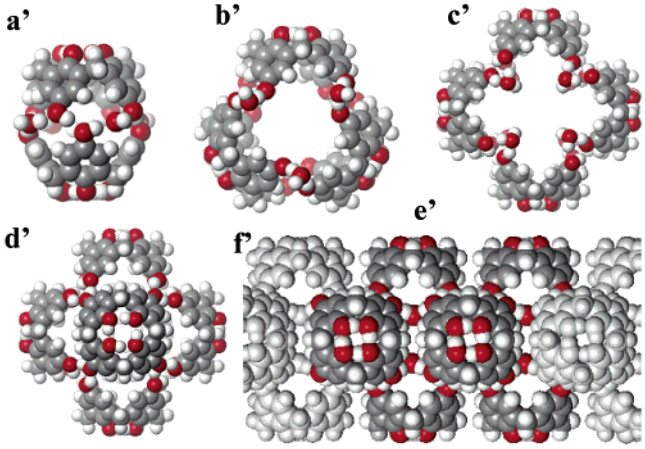

Figure 5. Space-filling model of oligomers in the presence of bridging water molecules: (a′) CHQ dimer, (b′) trimer, (c′) tetramer, (d′) hexamer, and (f′) tubular polymer with a repeating unit of tubular octamer (e′) which is highlighted in the mid region. Structures were obtained at the B3LYP/6-31G* level, while (f′) is constructed from the repeating units of (e′).

in the dimer, trimer, tetramer, hexamer, and octamer are 4, 6, 8, 0, and 16, respectively. The present conclusion does not depend on BSSE because the resulting relative assembling energies between these structures do not change significantly.

In the presence of water molecules, the CHQ oligomers can be better assembled by bridging water molecules which form H-bonds with unsaturated dangling H atoms. These H-bonds should provide lots of energy gain in the assembly of oligomers. Then, the tubular octamer (and polymers) gets large energy gain, while the hexamer without dangling H atoms has no energy gain in the presence of water. In the presence of bridging water molecules, the calculated assembling energies per monomer of the dimer, trimer, tetramer, hexamer, and octamer (Figure 5, Table 4) at the 50% BSSE-corrected B3LYP/6-31G* are 44, 40, 37, 22, and 47 kcal/mol, respectively. The calculations indicate that in the presence of water molecules, the assembling energy of the tubular octamer relative to the two tetramers is enhanced because of additional eight H-bonds between HQ and water (i.e., 47−37 = 10 kcal/mol-monomer). When the tubular octamer forms a linear chain with repeating units, the stability is further enhanced by almost the same amount (∼10 kcal/mol-monomer) with the formation of H-bonds between repeating units via bridging water molecules. These results are strongly in favor of the formation of tubular polymeric structures. Indeed, in experiments, addition of water molecules into CHQ in acetone resulted in a stable self-assembling tubular structure,[29] in agreement with the theoretical prediction. A similar tubular structure was also noted upon electrochemical reduction in the presence of water.

(28) The difference between the two calculations is because the 3-21G basis set gives much shorter H-bond lengths than the 6-31G* basis set. Thus, B3LYP/3-21G calculations need to be used with full BSSE correction, while B3LYP/6-31G* calculations are likely to be more realistic when 50% BSSE correction is employed.[6,26,27]

(29) In our experiments, the dimers which are almost as stable as (though slightly less stable than) the octamer (while much less stable than the almost insoluble long chain polymer with repeating units of octamer) seem to be present in a large quantity as the aqueous suspension.

Table 5. Interaction Energies (kcal/mol) and O···H Distances (Å in Parentheses) of the Three H-Bonding Types in Figure 6[a]

H-bonding	a. W>HQ_m	b. HQ_m>HQ_m	c. HQ_m>W
PM3	−2.34 (1.83)	−5.23(1.84)	−3.84 (1.80)
B3LYP/3-21G	−10.3 ± 6.1 (1.81)	−11.9 ± 5.4 (1.69)	−15.4 ± 4.9 (1.62)
	[−4.2]	[−6.5]	[−10.5]
B3LYP/6-31G*	−5.9 ± 1.7 (1.98)	−6.3 ± 1.5 (1.90)	−8.2 ± 1.2 (1.84)
PW-DFT	−6.0(2.01)	−4.2(1.90)	−7.9(1.82)
MP2/6-31G*	−5.9 ± 1.8 (2.01)	−8.3 ± 2.2 (1.92)	−8.1 ± 1.3 (1.87)
MP2/aug-cc-pVDZ[b]	−4.9 ± 0.7	−9.8 ± 2.1	−6.5 ± 0.7
	[−4.2]	[−7.7]	[−5.8]
	W>HQ	(HQ>)W> HQ(>HQ)	
B3LYP/6-31G*	−5.4 (1.99)	−7.2 (1.86)[c]	

[a] PM3 energies were obtained without BSSE correction. The PW-DFT method is free from BSSE. All other interaction energies are given as a median value between BSSE-uncorrected and BSSE-corrected values with the error bar of 50%-BSSE. Full-BSSE-corrected energies are given in brackets. In the case of HQ>HQ (instead of HQ_m>HQ_m), the PW-DFT, B3LYP/6-31G*, and MP2/6-31G* H-bond interaction energies are −4.6, −6.3, and −7.8 kcal/mol. See the text for the pure H-bond energies which exclude the $\pi-\pi$ interaction energies present in the MP2 values for the HQ>HQ and HQ_m>HQ_m. [b] Single point calculation at the MP2/6-31G* geometry. [c] Values for the central H-bond (W>HQ) in the three H-bonds relay comprised of three HQs and one W. To avoid the complex $\pi-\pi$ interactions by conformational distortion, all the O atoms involving the short H-bonds are constrained to be on the same plane.

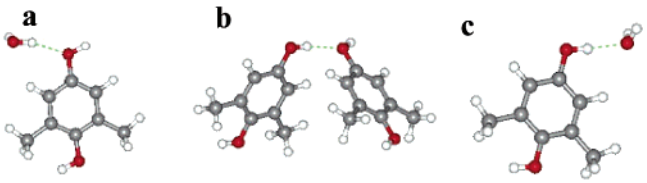

Figure 6. H-bonding types: (a) W>HQ_m, (b) HQ_m>HQ_m, and (c) HQ_m>W.

C. H-Bonding and Short H-Bonding. CHQ nanotubes involve three types of H-bonds represented as HQ_m>HQ_m, HQ_m>W, and W>HQ_m (Figure 6a−c), where the interactions between a proton donor (D) and a proton acceptor (A) will be denoted as D>A (where ">" represents the −OH bond orientation), and HQ_m and W denote dimethyl hydroquinone and water molecule, respectively. To better simulate the CHQ system, HQ_m as well as HQ was employed. The B3LYP/ 6-31G* H-bonding energies (with 50%-BSSE correction) of the three cases, W>HQ_m, HQ_m>HQ_m, and HQ_m>W, are 5.9, 6.3, and 8.2 kcal/mol, respectively (Table 5). These are similar to the corresponding PW-DFT values (6.0, 4.2, and 7.9 kcal/ mol) and full BSSE-corrected B3LYP/3-21G values (4.2, 6.5, and 10.5 kcal/mol, respectively), while the BSSE-uncorrected B3LYP/ 3-21G values are highly overestimated (16.4, 17.3, and 20.3 kcal/mol). The B3LYP/6-31G* H-bonding energies are also similar to the MP2/6-31G* values (5.9, 8.3, and 8.1 kcal/mol) and consistent to the MP2/aug-cc-pVDZ values (4.9, 9.8, and 6.5 kcal/mol) except for the overestimated HQ_m>HQ_m binding energy. In the HQ_m>HQ_m interaction, the MP2/6-31G* and MP2/aug-cc-pVDZ $\pi-\pi$ interaction energies (for the slanted pair) are 1.4 and 3.7 kcal/mol (which are not present in the B3LYP energies because of the lack of the dispersion energy), and so the pure H-bond energies are 6.9 and 6.1 kcal/ mol, respectively, which are close to the B3LYP/6-31G* HQ>HQ energy (6.3 kcal/ mol). In pure hydroquinone (HQ) instead of HQ_m, the HQ>HQ binding energy at the MP2/6-31G* level is 7.8 kcal/mol, and the pure H-bond energy is 6.4 kcal/mol, which is close to the B3LYP/6-31G* value (6.3 kcal/mol) and is in reasonable agreement with the PW-DFT value (4.6 kcal/mol). Though the pure H-bond energies of HQ>HQ at the MP2 and B3LYP levels are larger than that of PW-DFT level, the H-bond distance between the neighboring HQs is almost the same regardless of the levels of theory, because the H-bond for the HQ>HQ is present between two HQ moieties in the well-defined bell-shaped CHQ monomer structure comprised of four HQ moieties linked by the $-CH_2-$ groups. Thus, the HQ>HQ interaction energy would not affect the H-bond relay structure regardless of the levels of theory.

The MP2/6-31G* H-bond distances (O···H) in W>HQ_m, HQ_m>HQ_m, and HQ_m>W are 2.01, 1.92, and 1.87 Å, respectively. These are similar to the B3LYP/6-31G* values (1.98, 1.90, and 1.84 Å) and the PW-DFT values (2.01, 1.92, and 1.87 Å). However, B3LYP/3-21G predicts very short distances (1.81, 1.69, and 1.62 Å), which are almost consistently ∼0.2 Å smaller than other more accurate results. On the other hand, PM3 results (1.83, 1.84, and 1.80 Å) give no distinction between the three values, while the overall magnitude is better than the B3LYP/ 3-21G results, but it is still 0.1 Å smaller than the MP2 values. Thus, even though the B3LYP/3-21G gives short distances and large binding energies, the method reasonably describes the relative difference between different systems, which cannot be done properly in PM3 calculations. It is particularly interesting to note the clear differences in H-bond distance and H-bond energy between W>HQ_m and HQ_m>W. Compared with W>HQ_m, the HQ_m>W has shorter O···H distance (by 0.14 Å at both MP2/6-31G* and B3LYP/6-31G* levels) and larger binding energy (by 2.2 and 1.6 kcal/mol at MP2/6-31G* and MP2/aug-cc-pVDZ levels, respectively). The atomic charges (based on natural bond orbital population) of H and O atoms (q_H, q_O) involving H-bond for W>HQ are (0.49, −0.72) au, while those of HQ>W are (0.50, −0.94) au. Since the electrostatic energy which is the dominating component in the H-bond energy is proportional to the product of q_H and q_O, the HQ>W should have stronger binding energy than the W>HQ. This phenomenon is also noted from the water clusters, hydrated molecules, and their cations and anions.[27]

In nanotubes, we need to consider short H-bonds instead of the normal H-bonds which are common in many neutral H-bonded dimers. Therefore, the relay effect of additional H-bonds by HQs and water molecules (W's) should be taken into account. In the central H-bond of the three H-bonds relay comprised of HQ>W>HQ>HQ, the H-bond distance decreases by 0.2 Å with enhanced H-bond energy by ∼2 kcal/mol (from 5.4 to 7.2 kcal/mol). We also studied a nine H-bonds relay system of the fragment of the X-ray CHQ crystal (Table 6) using the PW-DFT optimized geometry. In the central region of this H-bonds relay system in the tubular CHQ polymer, the O···O distances of W>HQ, HQ>HQ, and HQ>W are 2.70, 2.68, and

2.66 Å at the PW-DFT level with the corresponding chemical shifts of 9.74, 11.97, and 12.44 ppm, respectively (Table 7). For the infinitely long H-bonds relay system of the CHQ crystal, the three distances are 2.61, 2.56, and 2.58 Å at the PW-DFT level (Table 6), which are slightly shorter (by ~0.08 Å) than but in reasonable agreement with the corresponding X-ray data (2.67, 2.64, and 2.67 Å). A similar size of deviation of the DFT calculated distances from the X-ray data was noted in our previous study of the H-bonds in ketosteroid isomerase.[12]

In the CHQ system, the H-bond energy with the increasing number of H-bonds does not show smooth increase because of distorted conformations by $\pi-\pi$ interactions. To obtain a more reliable H-bond relay effect in the linear system which does not involve other interactions, we have carried out the linear H-bonds relay system comprised of CHOH═CHOH molecules. From the investigation of B3LYP/6-31G* H-bond energies, the normal H-bond energy for the dimer is 5.9 kcal/mol, and the H-bond energies for the tetramer and decamer are 7.8 and 9.6 kcal/mol, respectively. The asymptotic value is ~9.9 kcal/mol, and the H-bond energy gain of the infinite H-bonds relay over the normal H-bond is ~4.0 kcal/mol.

Since the binding energy gain due to the SHB (~4 kcal/mol) is large, we investigated the atomic charges of H and O atoms involving the donor−acceptor H···O bond pair in the dimers and the nine H-bonds relay, on the basis of the natural bond orbital population analysis at the B3LYP/6-31G* level. In HQ>W, the charges of H and O (q_h, q_o) involving the H···O H-bond are (0.500, −0.943) au with charge enhancement by (0.017, −0.010) au with respect to the isolated HQ and W. In the nine H-bonds relay system, the (q_h, q_o) is (0.530. −0.987) au, with the charge enhancement by (0.046, −0.054) au which is much larger than those in the dimer system. Thus, the large energy gain in the short H-bond arises from the strong polarization effect along the H-bonds relay chain. It is also correlated to the H-bond length and chemical shifts. Shorter H-bonds show very large chemical shifts (up to 12.44 ppm for HQ>W in the central region of the nine H-bonds relay at the PW-DFT geometry similar to the X-ray geometry). The predicted chemical shift for the infinitely long 1-D H-bonds relay (which would be slightly larger than 12.44 ppm) is much larger than that for the four-membered circular H-bonds (9.37 ppm) in the CHQ monomer (i.e., by much more than 3.1 ppm).

The increase of the H-bonding energy in the H-bonds relay system is in agreement with the results of Dannenberg and co-workers[30] who studied the H-bonded formamide chains for which the H-bonds (RC═O···ROH type) are much stronger than the present case (ROH···HOH and ROH···ROH types). They reported that the bond energy can increase approximately twice the normal H-bond energy in the central region of long H-bonded formamide chains. Such enhancements in H-bonds relay system by bond polarization have been discussed by Salahub and co-workers.[31] The H-bonds relay effect (by adjacent tyrosine residues) also play an important role in increasing the enzyme reactivity.[12a]

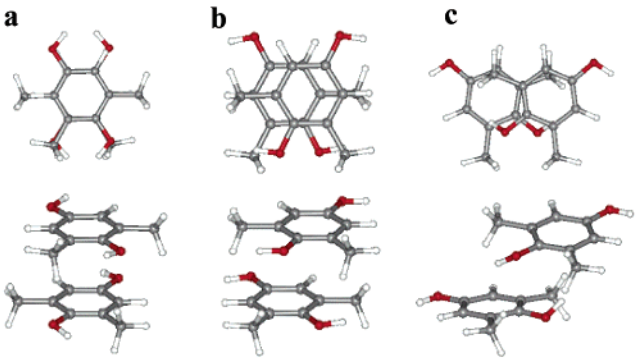

Figure 7. Displaced and parallel $\pi-\pi$ stacking: (a) parallel stack, (b) displaced stack with the interplanar distance fixed at 3.4 Å according to the X-ray structure, and (c) optimized displaced stack.

Table 6. Interoxygen Distances [and OH Distances and OH···O Angles], Two Types of O−O−O Bond Angles, and O−O−O−O Torsional Angles in the Infinite 1-D H-Bonds Relay of CHQ Crystals[a]

	a. W>HQ	b. HQ>HQ	c. HQ>W
X-ray1	2.664	2.661	2.664
	111,115/−112	117,115/101	115,111/112
X-ray2	2.683	2.628	2.683
	109,115/−110	115,116/101	116,109/110
X-ray$_{av}$	2.674	2.645	2.674
	110,115/−111	115,116/101	116,110./ 111
PW-DFT	2.61[1.61,176]	2.56[1.56,176]	2.58[1.58,173]
	115,121/−107	121,117/101	117,115/116

[a] Distances in Å; angles in degrees.

While the X-ray structure gives the same O···O distances (2.67 Å) for both W>HQ and HQ>W (because of the averaging of the distances because of the half occupancy for H atoms as a donor or an acceptor), the calculations show that the latter has slightly shorter length than the former (by 0.03 Å). In the 1-D CHQ system, we find that the short H-bonds are ~0.25 Å shorter than the corresponding normal H-bonds from both X-ray structures and PW-DFT calculations. Though the X-ray O···O bond distances are slightly longer than that of SSHB (<2.6 Å),[12c] the present short H-bonds have some characteristics of SSHBs. On the basis of these results, the tubular polymers (Figure 5f′) can easily grow with enhanced H-bonding energy (by 4 kcal/mol for each bond on the basis of PW-DFT calculations), which will be discussed in the latter section. Thus, four pillarlike building frames of 1-D short H-bonds[3] would help form single nanotubes in the assembly process of CHQs.

D. Displaced/Parallel Stacking. In $\pi-\pi$ stacking interactions, both displaced and parallel $\pi-\pi$ stacking interactions (Figure 7) need to be considered. In this case, the dispersion interactions are very important. However, since these dispersion interactions are not taken into account in density functional calculations, the B3LYP and PW-DFT tend to give slightly negative binding energies for these $\pi-\pi$ stacks. Thus, we have studied them on the basis of MP2 results, in particular, using a large basis set (aug-cc-pVDZ). In the benzene dimer, the BSSE-uncorrected MP2/6-31G* bindine energy (2.0 kcal/ mol) and full BSSE-corrected MP2/aug-cc-pVDZ binding energy (2.4 kcal/mol) are consistent to the experimental binding energy (2.4 kcal/mol), while the BSSE-corrected MP2/6-31G* binding energy is negative (−0.04 kcal/mol) and the BSSE-uncorrected MP2/aug-cc-pVDZ//MP2/6-31G* binding energy is overestimated (3.5 kcal/mol).[32] Therefore, we investigate the present

(30) (a) Kobko, N.; Paraskevas, L.; del Rio, E.; Dannenberg, J. J. *J. Am. Chem. Soc.* **2001**, *123*, 4348−4349. (b) Dannenberg, J. J.; Haskamp, L.; Masaunov, A. *J. Phys. Chem. A* **1999**, *103*, 7083−7086. (c) Masunov, A.; Dannenberg, J. J. *J. Phys. Chem. B* **2000**, *104*, 806−810. (d) Simon, S.; Duran, M.; Dannenberg, J. J. *J. Phys. Chem. A* **1999**, *103*, 1640−1643.
(31) (a) Guo, H.; Salahub, D. R. *Angew. Chem., Int. Ed.* **1998**, *37*, 2985−2990. (b) Guo, H.; Gresh, N.; Roques, B. P.; Salahub, D. R. *J. Phys. Chem. B* **2000**, *104*, 9746−9754.

Table 7. Proton Chemical Shifts (δ in ppm) Involving the H-Bond [HF/6-31G*//B3LYP/6-31G*(GIAO) Level]

W	HQ_m	W>HQ_m	HQ_m>HQ_m	HQ_m>W
1.18	3.80	3.75	6.78	7.12
(W>)HQ>W(>HQ>W)			(W>HQ>)W>HQ(>W)	
8.80			6.49	

Central Region in a Fragment of CHQ crystal (9 H-Bonds Relay)

W>HQ	HQ>HQ	HQ>W
9.74	11.97	12.44

system in terms of BSSE-corrected MP2/aug-cc-pVDZ//MP2/6-31G* binding energy. We have considered three cases: (a) the parallel stacking (optimized under the constraint that two HQ_m's are coaxial), (b) the displaced stacking (optimized under the constraint that the interplanar distance between two aromatic rings is fixed to the X-ray value, 3.4 Å), and (c) the displaced stacking (by full geometry optimization) at the MP2/6-31G* level. The BSSE-corrected MP2/aug-cc-pVDZ//MP2/6-31G* binding energies for the three cases, a, b, and c, are 7.9, 9.0, and 9.9 kcal/mol, respectively (Table 8).[33] Since case c includes weak H-bonding interactions between an O atom and a slightly positively charged H atom in a methyl group of HQ_m (employed to simulate the $-CH_2-$ group), it cannot represent pure stacking interaction shown in the CHQ structure. Case b which represents pure stacking interaction has the binding energy of 9.0 kcal/mol for the BSSE-corrected MP2/aug-cc-pVDZ//MP2/6-31G* (9.2 kcal/mol for the BSSE-uncorrected MP2/6-31G*). The potential energy surface of the stacking interaction is very flat, while the stacking energy is large (~9 kcal/mol). This HQ−HQ stacking energy is much larger than the benzene−benzene stacking energy (~2 kcal/mol for the displaced stacking). In HQ, the OH groups enhance the π electron density in the ring, but the two O atoms deplete the σ charges in the ring. This results in drastic reduction of electron exchange repulsion between π electron densities of two stacked HQs, since the π electron cloud of each HQ shrinks toward the HQ ring plane. Indeed, the interplanar distance between two stacked HQs (3.4 Å) is much shorter than that between two stacked benzenes (~4.0 Å)[32]. Therefore, in two stacked HQs, the dispersion energy drastically increases because of the shortened interplanar distance, resulting in large binding energy.

E. Geometrical and Electronic Structures of Calix[4]-hydroquinone Nanotube Crystal. We have performed electronic structure calculations of the CHQ crystal to understand the structures and electronic properties of nanotubes. Using the periodic boundary condition, the molecular structure has been fully optimized without imposing any symmetry constraints within a unit cell which is fixed to the X-ray characterized unit cell size. Since the positions of H atoms are not available in the X-ray structure, these were determined by PW-DFT calculations (Figure 8). These calculations clearly show not only infinitely long 1-D H-bond arrays composed of hydroxyl groups of CHQs and water molecules but also well-ordered intertubular $\pi-\pi$ stacking pairs. The calculated distance between two HQ centroids is 3.76 Å (interplanar distance: 3.54/3.48 Å) and the angle between two π-ring planes is only 3.5°, which are in good agreement with the experimental values (3.63 Å, 2.9°; interplanar distance: 3.41/3.38 Å) (Table 9). Even though PW-DFT does not properly take into account the $\pi-\pi$ interactions, the distance between two HQ centroids is in good agreement with the X-ray structure. Since in the PW-DFT approach the hard wall region is well described and the repulsion is small at the optimal contact length between two aromatic rings, the PW-DFT calculation reproduces well the crystal structure by the packing effect (which was obtained by fixing the unit cell size to the X-ray unit cell size). The agreement of the PW-DFT structure with the X-ray data is very good [monomer in Table 2, H-bonds in Table 6, and $\pi-\pi$ stacks (within the constraint of the X-ray crystal unit cell) in Table 9]. The calculated chemical bond lengths and angles are within 0.01 Å and 3 degrees from the X-ray data; the H-bond distances are only slightly shorter (within ~0.08 Å); the $\pi-\pi$ interplanar distances are only slightly larger (within ~0.1 Å).

In the 1-D H-bond arrays, the H-bond length is particularly short even in the absence of anionic charges. The O−O distance is 2.61 and 2.58 Å for the W>HQ pair and the HQ>W pair, and 2.57 Å for the HQ−HQ pair, (which are in reasonable agreement with experimental values of 2.67 and 2.64 Å, respectively), comparable to the SSHB length.[12] This indicates that the H-bond relay effect on the H-bond length is significant in the 1-D system. The predicted structure (with H atoms included) and the density of states (with respect to energy) are shown in Figure 8. The CHQ nanotubes are predicted to be an insulator with 2.9 eV band gap. The binding energy per short H-bond between HQ and W is calculated to be 10 kcal/mol,

(32) (a) Hobza, P.; Selzle, H. L.; Schlag, E. W. *J. Phys. Chem.* **1993**, *97*, 3937−3938. (b) Hobza, P.; Selzle, H. L.; Schlag, E. W. *J. Am. Chem. Soc.* **1994**, *116*, 3500−3506. (c) Hobza, P.; Selzle, H. L.; Schlag, E. W. *J. Phys. Chem.* **1996**, *100*, 18790−18794. (d) Jaffe, R. L.; Smith, G. D. *J. Chem. Phys.* **1996**, *105*, 2780−2788. (e) Tsuzuki, S.; Hobda, K.; Uchimaru, T.; Mikami, M.; Tanabe, K. *J. Am. Chem. Soc.* **2002**, *124*, 104−112.

(33) Since MP2 calculations using reasonably large basis sets (such as aug-cc-pVDZ) are known to give somewhat overestimated binding energy, full BSSE correction is desirable.[32] On the other hand, the BSSE-uncorrected MP2/6-31G* binding energies for case b (9.2 kcal/mol) are similar to those at the full BSSE-corrected MP2/aug-cc-pVDZ level (9.0 kcal/mol), whereas the full BSSE-corrected MP2/6-31G* binding energies (2.6 kcal/mol) are highly underestimated. This trend is also well noted in the benzene dimer calculations.[32] In MP2/6-31G*, the BSSE-uncorrected results are more realistic in obtaining the aromatic−aromatic interactions because of partial cancellation between the underestimated dispersion energy (due to insufficient basis set size) and the BSSE-driven overestimated interaction energy (which is again due to the insufficient basis set size).[6] Our experiences show that in H-bonding energy which is mainly electrostatic interaction (with insignificant dispersion energy), small basis sets such as 3-21G need full BSSE correction, while mid-size basis sets tend to give realistic values with 50% BSSE correction. On the other hand, in the aromatic−aromatic interactions with large dispersion energy, small basis sets such as 6-31G* underestimate the binding energies; thus they give better results without BSSE correction, while mid-size basis sets tend to give realistic values with 50% BSSE correction, and large basis sets require full BSSE correction because of overestimation of the interaction energy. In the DFT calculations (including B3LYP) of the aromatic−aromatic interactions, the hard wall region is well described, but the attractive well is often not found, since the binding energies tend to be repulsive (even though they are often slightly attractive because of BSSE). This is quite contrasted to the MP2 results or the reality. Nevertheless, the repulsive energy between two aromatic rings at the optimal interaction distance (on the basis of the X-ray structure and MP2 optimized structure) is insignificant (~1 kcal/mol), and furthermore the potential surface is almost flat regardless of the degree of displacement and the orientation of the aromatic rings. In MP2, the potential surface is also flat, while the binding energy is large. Thus, although the difference in binding energies between MP2 and DFT is large, this apparent difference would not raise serious problems in conformational analysis of systems involving other strong interaction forces, because the flat potential feature of the aromatic−aromatic interactions little affects the local conformation. This feature can often give reasonably reliable structures in calculations of crystal systems as long as the unit cell size is fixed to the experimental value. DFT results, when the unit cell size is fixed to that of the crystal, are in most cases in good agreement with X-ray structures, because the packing effect is predominantly determined by the van der Waals radii of atoms of molecules or exchange repulsions between molecules. However, the issue of dispersion force is important for determining the thermodynamic quantities of organic crystals having aromatic−aromatic interactions, which is a challenging subject.

Table 8. Interaction Energies and Interplanar Distances in $\pi-\pi$ Stacks[a]

	a. parallel	b. displaced (X-ray)[b]	c. displaced (optimized)
PM3	0.0 (∞)	1.4	−5.0
B3LYP/3-21G	1.3 ± 4.9 (3.71)	3.3 ± 5.1	
B3LYP/6-31G*	1.1 ± 1.3 (4.02)	3.6 ± 2.2	−1.9 ± 2.0
PW-DFT	0.0 (∞)	1.1	
MP2/6-31G*	−5.0 ± 3.2 (3.48)	−5.9 ± 3.3	−9.1 ± 3.3
MP2/aug-cc-pVDZ[c]	−12.1 ± 4.2 [−7.9]	−13.4 ± 4.4 [−9.0]	−14.5 ± 4.6 [−9.9]

[a] See the footnote of Table 4 for BSSE. Since the geometry was optimized at the BSSE-uncorrected energy surface, the BSSE-corrected B3LYP and DFT interaction energies can be positive as the two stacks are near the hard wall region because of the BSSE-driven interplanar distance shortening. The values in brackets are the full BSSE-corrected values. [b] In b, the interplanar distance of the displaced $\pi-\pi$ stack was fixed to the X-ray value (3.4 Å), while other geometrical parameters were optimized. [c] Single-point calculation at the MP2/6-31G* geometry.

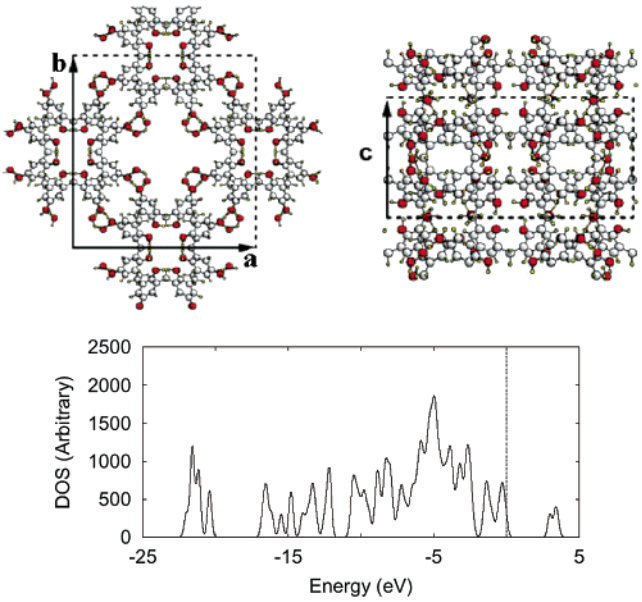

Figure 8. Calculated atomic structures (top and side views) and density of states (DOS) of CHQ nanotubes. The large white, small white, and dark spheres denote C, H, and O atoms, respectively. The unit cell is drawn by the dashed lines (a = 23.30 Å, b = 25.04 Å, c = 11.63 Å, and $\alpha = \beta = \gamma = 90°$). The HOMO energy is set to zero. The energy gap between HOMO and LUMO is 2.9 eV.

which is 4 kcal/mol larger than the average value (6 kcal/mol) of those of W>HQ, HQ>HQ, and HQ>W. The enhanced H-bond energy due to the formation of short H-bonds was obtained from the difference between the total interaction energy of the system with short H-bonds and the total interaction energy of a hypothetical system with the PW-DFT pair interaction energies (corresponding to normal H-bonds instead of short H-bonds). Namely, the nonadditive interaction energy was extracted from the PW-DFT calculations of these crystal systems, as often been used in the dissection of interaction energies in molecular cluster systems.[34]

F. Short H-Bonds and Displaced $\pi-\pi$ Stacks in CHQ Nanotube Bundles. In the absence of water, for each CHQ monomer, the number of dangling H atoms is 4, and the number of aromatic rings available for $\pi-\pi$ stacking interactions is also 4. Thus, four H-bond pairs and four $\pi-\pi$ stacking pairs can form by neighboring dangling H atoms and HQ rings of other CHQ monomers, respectively. As the $\pi-\pi$ stacking interactions are stronger than the normal H-bonds, the $\pi-\pi$ stacking would be favored. On the other hand, in the presence of water, the CHQs form chains HQ>(W>HQ>HQ>)$_n$W comprised of the

(34) Kim, K. S.; Dupuis, M.; Lie, G. C.; Clementi, E. *Chem. Phys. Lett.* **1986**, *131*, 451−456.

Table 9. Structure of Displaced $\pi-\pi$ Stack of CHQ Crystals[a]

	centroid – centroid	interplanar distance	off-center distance	off-axis angle	angle between two rings
X-ray1	3.630	3.413	1.237	19.94	2.86
		3.379	1.326	21.43	
X-ray2	3.624	3.403	1.247	20.11	2.92
		3.377	1.314	21.25	
X-ray$_{av}$	3.627	3.408	1.242	20.03	2.89
		3.378	1.320	21.34	
PW-DFT	3.759	3.535	1.277	19.88	3.53
		3.482	1.416	22.12	

[a] Distances in Å; angles in degrees.

building units (W>HQ>HQ>). Thus, per CHQ monomer in the CHQ nanotube bundles, each of two bridging water molecules involves two short H-bonds as a donor and an acceptor, and each OH group in a HQ moiety involves two H-bonds (one by the O atom and the other by the H atom). Since one bridging water molecule is present for two HQ moieties, the number of H-bond partners is three times the number of $\pi-\pi$ stacking partners. Although the strength of 1-D short H-bonding interaction (∼10 kcal/mol) is similar to the strength of the $\pi-\pi$ stacking interaction (∼9 kcal/mol), the assembling along the 1-D short H-bonds relay should be much more favorable because the number of H-bonds are three times the number of $\pi-\pi$ stacks. Indeed, in the presence of water, CHQs are assembled to form long tubular structures with four infinitely long short strong H-bond arrays (PW-DFT results in Figure 9a, b; X-ray results in Figure 9b′). This feature should be related to the high-resolution transmission electron microscope (HRTEM) image of a single nanotube of 2-nm width loosely bound to a CHQ bundle.[3a] In the absence of water, we see laminar filmlike structure of CHQs for which the numbers of both interaction pairs are the same, because the $\pi-\pi$ stacking interactions (∼9 kcal/ mol) are stronger than the normal H-bonding interactions (∼6 kcal/mol). The CHQ tubes assembled to form long tubular structures in the presence of water are grown into bundles with intertubular $\pi-\pi$ stacking interactions (PW-DFT results in Figure 9c, d; X-ray results in Figure 9d′), resulting in crystals with well-ordered two-dimensional arrays of pores (Figures 10 and 11). A similar phenomenon has been observed from atomic force microscope (AFM) images, as time evolves with reduction of CQ (to be published).

In the X-ray crystal structure,[3] 1 unit cell comprises 8 CHQ monomers (comprised of 32 HQ moieties) and 16 bridging water molecules, which involve 80 H-bonds (48 for four 1-D H-bond arrays and 32 for four circular four-membered H-bonds) and 16 $\pi-\pi$ stacking pairs, where the double count due to the neighboring HQ partners in other unit cells is removed. The number of H-bonds in the needlelike crystal is three times the

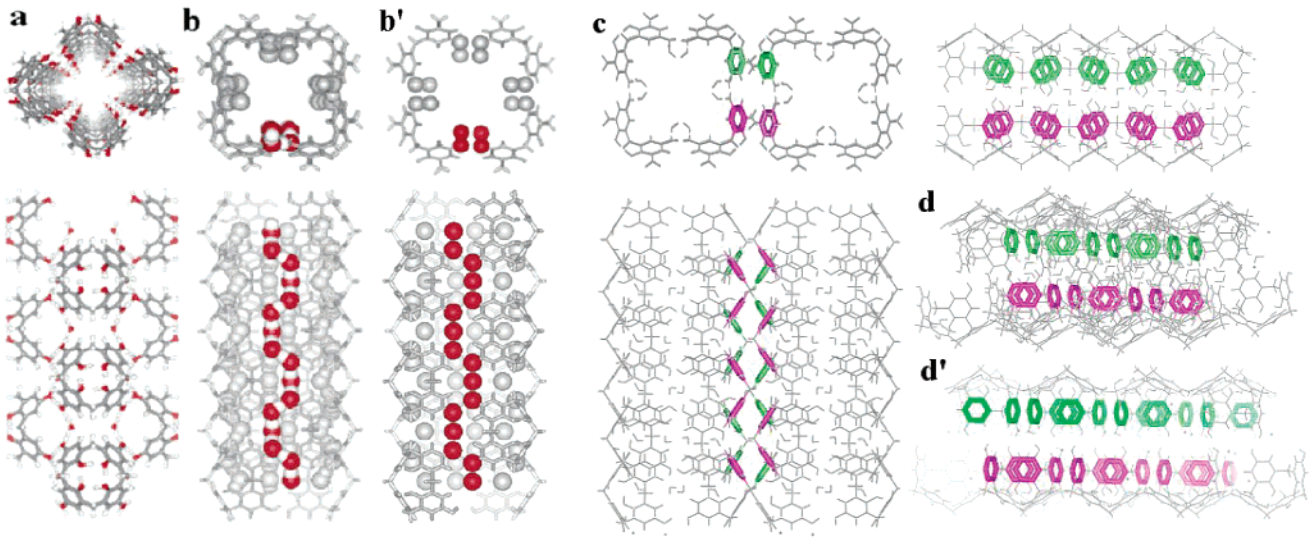

Figure 9. Longitudinal H-bond relay between CHQs and water molecules and intertubular $\pi-\pi$ stacking interactions: (a) Four pillar frames of short H-bonds (in red) are shown as the top view; (b) The space-filled part (with O atoms in red and H atoms in white) represents a 1-D H-bonds relay comprised of hydroxyl groups (−OH) and water molecules, where only 1-D H-bonds array is clearly represented for visual aid; (b′) the X-ray structure corresponding to (b); (c) Top view with two side views; (d) Projected view to show displaced stacks on aromatic rings plane; (d′) the X-ray structure corresponding to (d). Note the similarity in the position of heavy atoms between the X-ray and PW-DFT structures, while the H atom positions are not given in the X-ray structutres. Figures b′ and d′ clearly demonstrate the striking features of the infinitely long 1-D H-bonds arrays and the exemplary displaced $\pi-\pi$ stacks, respectively.

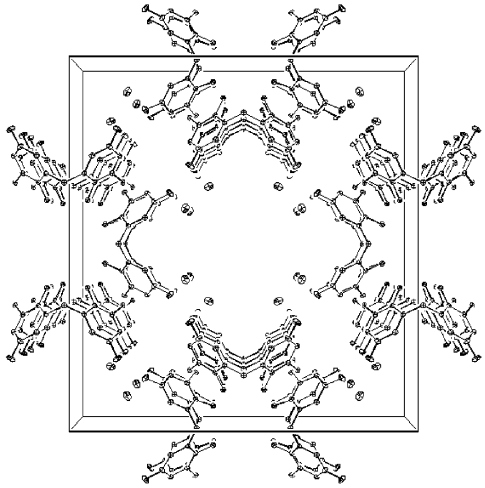

Figure 10. X-ray structures of CHQ nanotubes crystal.

number of $\pi-\pi$ stacking pairs. A nanotube bundle shows the infinitely long 1-D H-bonding network between hydroxyl groups of CHQs and water molecules and well-ordered intertubular $\pi-\pi$ stacking pairs (Figure 9). Figure 9d and 9d′ shows clear projected views of the $\pi-\pi$ stacks on the aromatic rings plane. The $\pi-\pi$ stacks in PW-DFT calculations (Figure 9d) are very close to the $\pi-\pi$ stacks in the X-ray structure (Figure 9d′). Thus, though the PW-DFT calculations do not properly take into account the $\pi-\pi$ interactions, the packing effect (by fixing the unit cell size to the crystal data) resolves such problems, and the overall structure (Figure 11) is in excellent agreement with the X-ray structure (Figure 10).

The self-assemblies of pure organic molecules hardly exhibit rectangular shapes and large pore sizes, whereas the bundles of CHQ nanotubes form very large and novel chessboardlike rectangular structures (Figure 11). The apparent size of each inner square channel (with the van der Waals volume excluded) is 6×6 Å^2 in terms of apparent cross section on the projected plane. However, the real cross section (with the van der Waals volume excluded) is 8×8 Å^2 because atoms are located in zigzag shape, and the shortest distance between one atom on a wall in the tube and another atom on the other side of the wall is 11 Å. An annealing technique[34] was employed to study the pore volume using classical molecular dynamics simulations (for 10 ps), as we studied in a membrane channel.[35] When it is fully solvated, it has about 48 water molecules in a unit cell, which corresponds to the volume of $8 \times 8 \times 11.63$ Å^3. The solvent-accessible surfaces are shown in Figure 11b.

To obtain the solution effect of the 1-D short H-bonds, we carried out PW-DFT calculations of the CHQ crystal in the explicit presence of solvent water molecules (48 water molecules in a unit cell excluding the bridging water molecules) with the periodic boundary condition for the X-ray crystal unit cell. In this case, the binding energy per short H-bond is evaluated to be 9 kcal/mol, as the nonadditive interaction energy was extracted from the PW-DFT results of both the real system with the nonadditive interaction energies and a hypothetical system with the PW-DFT pair interaction energies. The solvent effect reduces the short H-bond strength, but the effect is rather small (1 kcal/mol). More technical details of the PW-DFT calculations in which the solvent water is explicitly included and the details of the solvent structures in the present system will be reported elsewhere.

It is very important to know the surfaces and edges of the CHQ bundles, since this information is useful for understanding the gate phenomena of ion/water transport.[35] The surfaces and edges of CHQ bundles are clearly seen in Figure 12 along with Figure 9.

G. IR Spectra of Calix[4]hydroquinone Bundles. The 1-D H-bond relay effect should be significant in the IR spectra

(35) (a) Kim, K. S.; Nguyen, H. L.; Swaminathan, P. K.; Clementi, E. *J. Phys. Chem.* **1985**, *89*, 2870−2876. (b) Kim, K. S.; Clementi, E. *J. Am. Chem. Soc.* **1985**, *107*, 5504−5513. (c) Kim, K. S.; Vercauteren, D. P.; Welti, M.; Chin, S.; Clementi, E. *Biophys. J.* **1985**, *47*, 327−335.

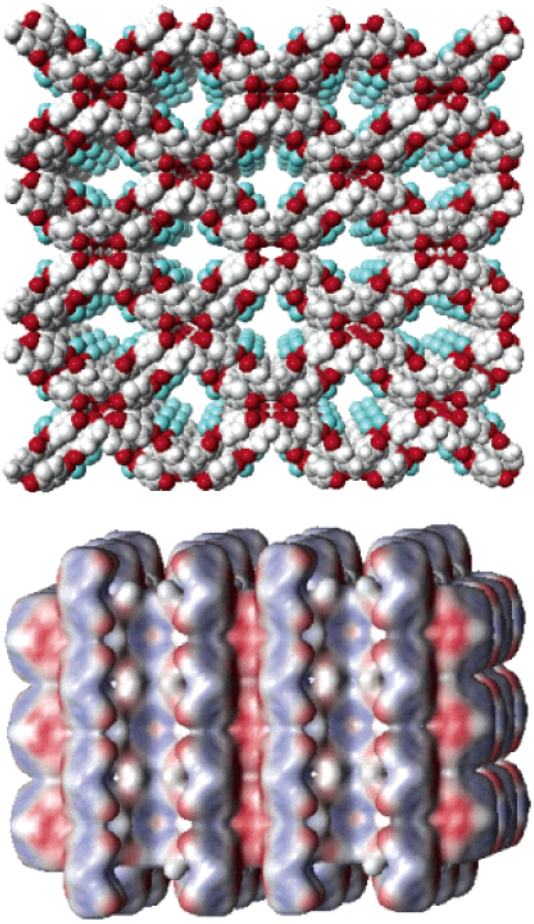

Figure 11. Cross-sectional views of the CHQ nanotube crystal structure with bridging water molecules: (a) perspective view (O of HQ in red; O of water in turquoise) and (b) side view showing solvent-accessible surface. The size of the pore (with the van der Waals volume excluded) is 6×6 Å^2 on the projected view. However, the actual pore size is 8×8 Å^2 because atoms are located in zigzag shape. The nearest distance between atoms on the opposite sides of the pore is 11 Å.

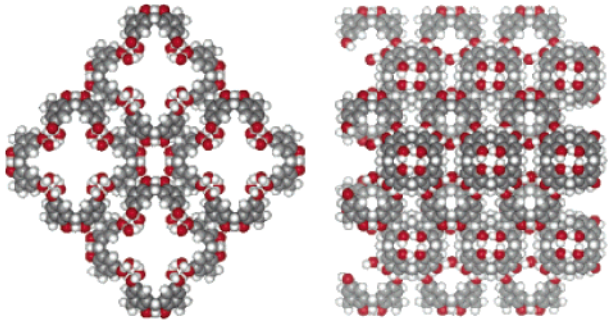

Figure 12. Surfaces and edges of the system comprised of four short nanotubes (top and side views).

(Figure 13). The FT-IR spectra of CHQ nanotubes show evidence of the strong H-bond networks. The experimental OH stretching vibration modes of the CHQ monomer consist of free and four-membered circular H-bonded OH vibrations (Figure 13a, b) around 3555 (3600 by deconvolution) and 3200 cm^{-1}, respectively, which are in good agreement with the B3LYP/6-31G* frequencies scaled by a constant 0.962 (3610 and 3200 cm^{-1}) or by exponential scaling.[36] The experimental frequency around 3388 (3400 in deconvolution) cm^{-1} seems to arise from the dimer conformation. In the tubular structures, the intensities

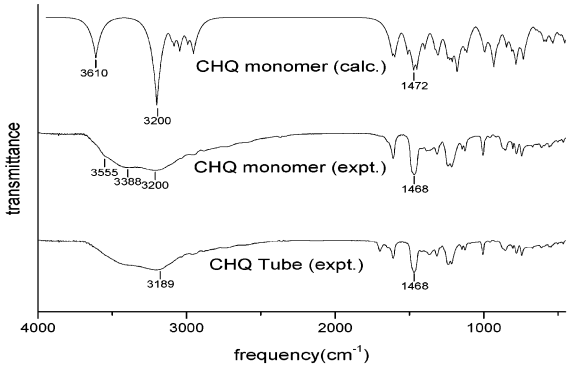

Figure 13. B3LYP/6-31G* and experimental IR spectra of the CHQ monomers, in comparison with the experimental IR spectra of CHQ tubes. The calculated frequencies were scaled by 0.962.

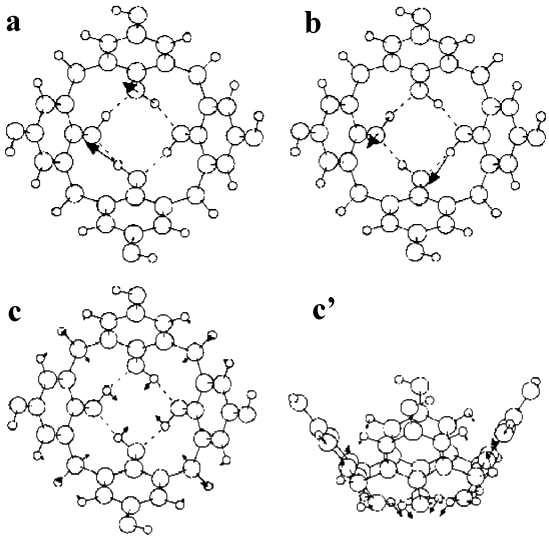

Figure 14. Mode Analysis of IR characteristic peaks of the CHQ monomer: (a, b) two degenerate modes corresponding to 3200 cm^{-1}, and (c, c′) top and side views of the mode 1468 cm^{-1} involving dipole change upon vibration. Other two degenerate modes corresponding to 3200 cm^{-1} do not involve dipole change by symmetry upon vibrational excitation, and thus they are IR-inactive.

of the free OH stretching vibration peak and partially dimerlike OH stretching peak decrease, while the H-bonded OH stretch mode shifts to 3189 cm^{-1}, indicating the formation of long tubular structures with strong 1-D short H-bond networks. In addition, the hydrogen breathing mode of the four-membered circular H-bonds of the cone is 1468 cm^{-1} (Figure 14 c, c′) from the mode analysis.

IV. Concluding Remarks

We have shown how the arrays of CHQ nanotubes were designed from computer-aided molecular design approach so that this method can be utilized to design other functional molecular systems. We have investigated the 1-D short H-bonds and the displaced $\pi-\pi$ stacking interactions in the CHQ nanotube bundles and their competitions in the assembling process.

According to ab initio calculations, the most stable conformers of CQ and CHQ are "partial cone" and "cone" structures,

(36) (a) Lee, J. Y.; Hahn, O.; Lee, S. J.; Choi, H. S.; Shim, H.; Mhin, B. J.; Kim, K. S. *J. Phys. Chem.* **1995**, *99*, 1913−1918. (b) Lee, J. Y.; Hahn, O.; Lee, S. J.; Choi, H. S.; Mhin, B. J.; Lee, M. S.; Kim, K. S. *J. Phys. Chem.* **1995**, *99*, 2262−2266.

respectively. CHQ is composed of four HQ moieties, therefore, it has eight hydroxyl groups. Among them, four inner hydroxyl groups form a circular proton-tunneling resonance of H-bonds which stabilize the "cone" structures, and the other four hydroxyl groups in the upper rim of the cone have dangling H atoms, which make it possible to form intermolecular H-bonds that lead to self-assembled structures. In *n*-oligomers of CHQ, the number of OH groups is 8*n*, and thus, 4*n* OH groups form *n* cones comprised of four-membered circular H-bonds, and the remaining 4*n* OH groups can involve intermolecular H-bonds. Full saturation of the dangling H atoms in *n*-oligomer can be accomplished with 4*n* H-bonds. Since the octahedral hexamer forms 24 H-bonds with full saturation of dangling H atoms, it has the largest assembling energy among the possible assembling structures. However, in the presence of water molecules, other CHQ oligomers can be better assembled by bridging water molecules involving H-bonding with unsaturated dangling H atoms, with lots of energy gain in the assembly process. Then, in the presence of water, the tubular polymer is the most stable with the formation of four infinitely long short H-bonding pillarlike frames along the repeating units via bridging water molecules.

To better understand the short H-bonds and the displaced $\pi-\pi$ stacks, we carried out X-ray characterization of two crystals grown in different conditions. The structure of CHQ tubes, which have exemplary displaced $\pi-\pi$ stacks as well as the infinitely long 1-D short H-bonds arrays, have been well refined. The bond lengths of the infinitely long short H-bonds are 2.64−2.67 Å, and the interplanar distance between two displaced $\pi-\pi$ stacks is 3.4 Å. The average interaction energy of longitudinal short H-bonds in the CHQ nanotubes is 10 kcal/mol, in contrast to 6 kcal/mol for normal H-bond interaction energy. The solvent water reduces the short H-bond strength by only 1 kcal/mol, and the average interaction energy of short H-bonds is 9 kcal/mol. These short H-bonds have some characteristics of the well-known SSHB. Their energy gain is due to charge polarization, while SSHB has an additional energy gain by charge dissipation.[12b] The intertubular interaction forces to form a nanotubes bundle arise mainly from parallel displaced aromatic−aromatic stacking interactions. The calculated energy for an aromatic stacking pair is ∼9 kcal/mol which is much greater than that in the benzene dimer (∼2 kcal/mol). In the presence of bridging water molecules, the number of H-bonding pairs is three times that of $\pi-\pi$ stacking pairs. Thus, the 1-D linear tubular growing is more favored than the assembling of tubes into a bundle.

IR spectroscopic characterization (∼3190 cm^{-1} along with normal-mode analysis) and the NMR chemical shifts measurements of four-membered circular H-bonds in the cone of the CHQ monomer have been made. The chemical shift of the infinitely long short H-bonds is predicted to be (slightly) larger than 12.4 ppm, which is at least 3 ppm larger than that of four-membered circular H-bonds in the cone of the CHQ monomer moiety. On the basis of the first principles calculations (PW-DFT) of the self-assembled CHQ nanotube crystal, we determined the position of H atoms which are absent in the X-ray data but are essential for understanding the features of 1-D H-bonding. The density of states of CHQ was studied, and the energy band gap (2.9 eV) was evaluated.

We have assessed the utility of various calculation methods that we employed for the design of the CHQ nanotubes and the understanding of the corresponding assembly process. To predict functional molecular systems and investigate self-assembling phenomena with the computer-aided design approach (i.e., for the minimal quantitative analysis of the present system), B3LYP/6-31G* is recommended for the study of H-bonds, while the $\pi-\pi$ interactions need to be employed at least at the BSSE-uncorrected MP2/6-31G* level or preferable at the BSSE-corrected MP2/aug-cc-pVDZ level.

The present organic nanotubes would be used as a model for selective water/ion channels in biological systems using cation$-\pi$ interactions[37] and as a nanoreactor for specific chemical transformations (i.e., as a nanohost). The infinitely long 1-D H-bond arrays in the nanotube are expected to have interesting features in long-range proton-tunneling phenomena[20] and other physical/chemical properties. As the HQ moiety is a powerful reducing agent for metal ions and can form charge-transfer complexes with electron-deficient molecules, this novel characteristic is useful for designing nanosize metal structures (clusters, rods, and wires) on the basis of nano-recognition.[38] The interesting redox feature of CHQ has been applied to the design of electrochemically controlled nanomechanical devices like the molecular flipper.[39] Thus, the unusual structures and functions of CHQ nanotubes can be employed in diverse fields of chemistry, biology, and material science.[40]

Acknowledgment. This research was supported by KISTEP(CRI) and partly by BK21.

Supporting Information Available: Two X-ray data of CHQ crystals grown in the presence of Cs_2SO4 and NMe_4PF_6 and the calculated energies and structures of the CHQ monmer, dimer, trimer, tetramer, hexamer, and octamer without and with bridging water molecules. This material is free of charge via the Internet at http://pubs.acs.org.

JA0259786

(37) (a) Dougherty, D. A.; Stauffer, D. *Science* **1990**, *250*, 1558−1560. (b) Kumpf, R. A.; Dougherty, D. A. *Science* **1993**, *261*, 1708−1710. (c) Dougherty, D. A. *Science* **1996**, *271*, 163−168. (d) Ma, J. C.; Dougherty, D. A. *Chem. Rev.* **1997**, *97*, 1303−1324. (e) Kim, K. S.; Lee, J. Y.; Lee, S. J.; Ha, T.-K.; Kim, D. H. *J. Am. Chem. Soc.* **1994**, *116*, 7399−7400. (f) Lee, J. Y.; Lee, S. J.; Choi, H. S.; Cho, S. J.; Kim, K. S.; Ha, T. K. *Chem. Phys. Lett.* **1995**, *232*, 67−71. (g) Choi, H. S.; Suh, S. B.; Cho, S. J.; Kim, K. S. *Proc. Natl. Acad. Sci. U.S.A.* **1998**, *95*, 12094−12099. (h) Carbacos, O. M.; Weinheimer, C. J.; Lisy, J. M. *J. Chem. Phys.* **1998**, *108*, 5151−5154. (i) Carbacos, O. M.; Weinheimer, C. J.; Lisy, J. M. *J. Chem. Phys.* **1999**, *110*, 8429−8435.

(38) The nanosize metal structures are self-synthesized by the electrochemical redox process. The species involved in the self-synthesis (i.e., spontaneous nano-recognition driven chemical synthesis) lose their original chemical identity to form well-ordered nanostructures unlike the self-assembly which maintains the chemical identity of building blocks.[3c]

(39) Kim, H. G.; Lee, C.-W.; Yun, S.; Hong, B. H.; Kim, Y.-O.; Kim, D.; Ihm, H.; Lee, J. W.; Lee, E. C.; Tarakeshwar, P.; Park, S.-M.; Kim, K. S. *Org. Lett.* **2002**, in press.

(40) The self-assembly of CHQ nanotubes by the molecular recognition involving H-bonding and π-π interactions can be simply compared to magnetic legos which can be self-assembled into toys.